# Comparison of Atomic-Level and Coarse-Grained Models for Liquid Hydrocarbons from Molecular Dynamics Configurational Entropy Estimates

**Riccardo Baron,[†] Alex H. de Vries,[†,‡] Philippe H. Hünenberger,[†] and Wilfred F. van Gunsteren*,[†]**

*Laboratorium für Physikalische Chemie, ETH-Zürich, CH-8093 Zürich, Switzerland, and MD group, Department of Biophysical Chemistry, University of Groningen, Nijenborgh 4, 9747 AG Groningen, The Netherlands*

*Received: October 14, 2005; In Final Form: February 7, 2006*

Molecular liquids can be modeled at different levels of spatial resolution. In atomic-level (AL) models, all (heavy) atoms can be explicitly simulated. In coarse-grained (CG) models, particles (beads) that represent groups of covalently bound atoms are used as elementary units. Ideally, a CG model should reproduce the thermodynamic and structural properties of the corresponding AL model after mapping to the lower-resolution scale. In the present work, two such models are investigated: (i) the classical GROMOS atomic-level model; (ii) a CG model recently proposed by Marrink et al., which maps approximately four non-hydrogen atoms to one bead [*J. Phys. Chem. B* **2004**, *108*, 750]. The study is restricted to *n*-alkanes whose aliphatic fragments are abundantly found in lipids of biological interest. Additionally, *cis*-9-octadecene is included, as a template chain of the lipid dioleoylphosphatidylcholine (DOPC). The two representations of molecules in the liquid phase are compared in terms of average molecular structures, extent of configurational space sampled, and single-molecule entropies. An approximate method is used to estimate the rotational contributions to the absolute configurational entropy. Good correspondence between the AL and CG representations is found. The loss in configurational entropy due to the reduction in degrees of freedom upon coarse-graining of the model is estimated.

## Introduction

In recent years, there has been a steadily growing interest in the development of coarse-grained (CG) models for a variety of polymers (for reviews, see refs 2, 3, and 4) and for systems consisting of lipids and surfactants (for reviews, see refs 5 and 6). Different from the classical atomic-level (AL) representations, these models consist of beads (also called superatoms or interaction sites with mass) representing groups of atoms, monomers, or even several monomeric units. These beads interact through an effective potential energy function (force field) that takes into account the effect of the omitted degrees of freedom in a mean-field manner. Models of this type have originally been proposed by Smit et al. to study a water−oil interface in the presence of micelles[7] as well as surfactant self-assembly.[8] The possibilities of extending this approach to polypeptide and nucleic-acid systems are more limited, because many different types of CG beads would be required in this context to account for the specific physicochemical properties of individual groups (e.g., side chains in proteins, bases in nucleic acids). Therefore, only a reduced number of studies have been reported for these types of biomolecules (for a comprehensive review on coarse-grained models for proteins, see ref 9). On the contrary, several approaches have been followed with success to arrive at semiquantitative CG descriptions of the properties of lipids,[1,10−12] DPPC-cholesterol bilayers,[13] amphiphilic di-block copolymers,[14] and solvated malto-oligosaccharides.[15]

The use of CG models is complementary to a more accurate AL description. With a CG model, the size-scale and time-scale dependence of the system properties can be explored,[16−20] while the investigation can be followed by a focused atomistic study of important details using an AL model. This is an appealing procedure, for instance, when a long AL molecular dynamics simulation would be excessively expensive and/or to obtain equilibrated atomistic structures for slowly relaxing systems. In the latter case, the system can be constructed and equilibrated using the CG model and, subsequently, mapped to an AL model. Simulations using the latter model then need to be equilibrated only for a comparatively short simulation time and can be used to compute thermodynamic, dynamic, and structural properties that require atomistic detail. To achieve consistency, however, the CG model should reproduce the most relevant features of the AL model and cannot be considered as an independent substitutive tool. In practice, the quality of a CG model mainly depends on the chosen coarse-graining procedure, including (i) the model resolution (how many AL particles per CG bead), (ii) the mapping procedure (how the bead positions are defined as a function of the AL particle coordinates), (iii) the potential energy function entering into the CG Hamiltonian, and (iv) the experimental and AL simulation properties against which the CG model parameters are optimized.

Irrespective of the chosen coarse-graining procedure, the average molecular structure and flexibility are among the properties which should be considered when validating a CG model by comparison with corresponding AL simulations. Average molecular structures at the CG and AL levels can easily be compared.[15,17] Flexibility at the two levels can be compared by examining the configurational spaces sampled by the two

* Corresponding author. Tel.: +41-1-6325501. Fax: +41-1-6321039. E-mail: wfvgn@igc.phys.chem.ethz.ch.
[†] Laboratorium für Physikalische Chemie, ETH-Zürich.
[‡] University of Groningen.

10.1021/jp055888y CCC: $33.50 
Published on Web 04/04/2006

models. In addition, the thermodynamic properties of both types of models should be comparable. Here, we investigate more specifically the corresponding configurational entropies.

The configurational entropy is a thermodynamic quantity directly related to the accessible configurational space of a molecular system (i.e., for a single-molecule, to its flexibility). The reliable estimation of entropies and entropy differences from molecular dynamics (MD) simulations is a notoriously difficult problem that currently constitutes one of the key challenges in computational chemistry.[21−30] This is because the absolute entropy is a measure of the overall extent of phase space accessible to a system and can thus in principle only be determined on the basis of an infinitely long simulation. A method to estimate configurational entropies from MD trajectories was first introduced by Karplus and Kushick,[21] by postulating a multivariate Gaussian probability distribution associated to the nondiffusive degrees of freedom of a molecular system (quasi-harmonic assumption). Implications for free energy determination as well as the effects of constraints, coordinate transformations, and quantum corrections were later provided, together with a critical analysis of the approximations involved in the quasi-harmonic approach and of the resulting errors.[22,23,30] Two variants of the quasi-harmonic analysis in Cartesian coordinates have been suggested. In the most recent version of Andricioaei and Karplus,[26] the quasi-harmonic entropy is estimated by diagonalizing the covariance matrix and applying the exact quantum-mechanical equation for the entropy of a one-dimensional harmonic oscillator to the corresponding eigenvalues. In the original approach of Schlitter,[24] the diagonalization process is substituted by a determinant calculation and the correct quantum-mechanical formula for the entropy is replaced by an approximate heuristic expression. In practice, the two alternative formulations result in very similar (2% different) entropy estimates.[29,30]

Here, the (single-molecule; see Table 1) configurational entropy of pure hydrocarbons in the liquid state is estimated. Two models are investigated. In the GROMOS AL model,[31−33] each atom in a molecule is represented by one interaction site, except aliphatic groups, for which the carbon atom and bound hydrogen atoms (united atom) are treated as one interaction site. This united-atom force field reproduces the properties of *n*-alkanes as accurately as all-atom (i.e., explicitly including all hydrogen atoms) force fields.[34] The second model is the coarse-grained (CG) model recently proposed by Marrink et al.,[1] which approximately maps four non-hydrogen atoms to one interaction site (bead) and has been optimized to model lipid aggregates in water.

The set of hydrocarbons considered here has been chosen with an eye to the occurrence of aliphatic chains in lipids of biological interest. The molecule sizes have been limited to *n*-alkanes up to hexadecane (Figure 1) and octadecane, which allows for comparison with available experimental data. Additionally, *cis*-9-octadecene (Figure 1) was included in the set in order to investigate the effect of the central double bond in both the AL and CG models and for its relevance as a template for dioleoylphosphatidylcholine (DOPC), a lipid occurring in biological membranes.

By estimating configurational entropies, the present work addresses several aspects concerning the simplification of a force field for MD simulations. First, what is the simulation length required for a single hydrocarbon molecule to sample its accessible configurational space? Is it possible to measure the extent of the configurational space sampled and to estimate the entropy contribution associated with single-molecule overall rotation? Second, to what extent does the CG model reproduce the properties of the AL model in terms of entropy, dynamics, and structure? Vice versa, how does the AL description map to the CG picture?

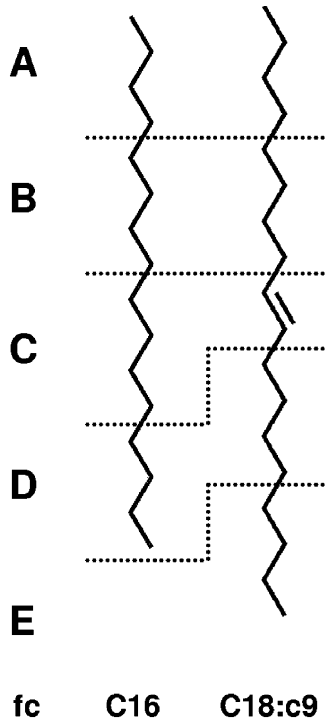


**Figure 1.** Definition of the fragments (fc = A, B, C, D, or E) of hydrocarbon chains for hexadecane (C16) and *cis*-9-octadecene (C18:c9). The dotted lines indicate fragment boundaries. Fragments are used to map the atomic-level (AL) model onto the coarse-grained (CG) model.

## Methods

**Molecular Dynamics Simulations.** Trajectories for liquid hydrocarbons were generated using the MD package GROMACS (version 3.0, ref 35) based on either the AL (GROMOS 45A3, ref 32) or the CG (ref 1) force fields. All systems were simulated under rectangular periodic boundary conditions. The weak-coupling algorithm[36] was used to maintain a constant average temperature (at a specified reference value) and pressure (at 1 atm), with relaxation times of 0.1 and 0.5 ps, respectively, and an isothermal compressibility of $4.6 \times 10^{-4}$ kJ$^{-1}$ mol nm$^3$. All MD simulations were initialized with atomic (AL) or bead (CG) velocities taken from a Maxwell−Boltzmann distribution at the desired temperature. Newton's equations of motion were integrated using the leapfrog algorithm[37] with time steps of 5 (AL) or 40 (CG) fs. The overall system center of mass translation and rotation was removed at every step. In the AL model, the bond lengths were constrained using the LINCS algorithm[38] with a relative geometric tolerance of $10^{-4}$ and the nonbonded (exclusively Lennard−Jones) interactions were truncated at a distance of 1.2 nm. The CG model differs from the AL model in that (i) no constraining procedure is applied to (pseudo) bond lengths (which are described by harmonic springs), (ii) Lennard−Jones interactions between second (pseudo) neighbors are not excluded, and (iii) for the Lennard−Jones potential energy term the standard GROMACS shifting function[35] is used between 0.9 nm and the cutoff distance of 1.2 nm. Simulations of five different hydrocarbons were performed using the AL model, consisting of 128 molecules of dodecane (*n*-$C_{12}H_{26}$, C12), tetradecane ($C_{14}H_{30}$, C14), hexade-

**TABLE 1: Comparison of the Concepts of Molecular and Single-Molecule Entropies**

| | molecular entropy | single-molecule entropy |
|---|---|---|
| experiment | 1 mol of pure liquid, standard pressure 1 bar, specified temperature | NOT accessible |
| simulation | NOT accessible | single liquid molecule surrounded by bulk liquid,[a] specified temperature |
| entropy contributions | single-molecule internal,[b] single-molecule rotational,[b] single-molecule translational,[c] intermolecular correlations[d] | single-molecule internal,[b,e] single-molecule rotational, [b,f] [single-molecule translational[c]] |

[a] Due to the mean effect of interactions with the surrounding molecules, the single-molecule entropy in the liquid state is not identical to the entropy of a single molecule in a vacuum. [b] The separation of internal and rotational contributions cannot be done unambiquously because of their coupling through the inertia tensor of the molecule. [c] The ideal-gas contribution, which can be evaluated analytically through the Sackur−Tetrode equation based on the molar volume of the liquid at the standard pressure of 1 bar and the given temperature, was not evaluated in the present study. [d] Involve the three types of single-molecule degrees of freedom (internal, rotational, and translational); These are currently not accessible from simulations. [e] Approximately accessible (upper bound) from simulations through quasi-harmonic analysis using coordinates translationally and rotationally fitted to a reference structure; This contribution neglects mode anharmonicity and mode correlations (beyond pairwise linear ones) within the single molecule. [f] Approximately accessible (upper bound) from simulations through quasi-harmonic analyses with and without rotational fitting; This contribution neglects the highly correlated nature of rotational motion and could also be estimated from the quantum-mechanical entropy of a rigid rotor based on the average inertia tensor from the simulation.

cane ($C_{16}H_{34}$, C16), octadecane ($C_{18}H_{38}$, C18), and *cis*-9-octadecene ($C_{18}H_{36}$, C18:c9). Corresponding simulations using the CG model were only performed for pure hexadecane and *cis*-9-octadecene. In this case, larger systems of 256 or 512 molecules were simulated.

Initial configurations for both types of models were generated at the experimental density (liquid phase at the specified temperature), by randomly attributing particle positions while avoiding particle overlaps and crossing of the hydrocarbon chains. An initial equilibration phase of 1 (AL) or 10 (CG) ns was followed by sampling simulations over up to 200 ns (AL) or 1 $\mu$s (CG). The entire sampling periods were used for analysis. Unless otherwise specified, analysis results are averaged over all hydrocarbon chains in the simulated liquid sample.

**Entropy Calculations.** Configurational entropy calculations were performed following the formulation of Schlitter.[24] This analysis provides an approximate value (upper bound) $S$ to the true configurational entropy $S_{\text{true}}$ of the simulated system,

$$S_{\text{true}} < S = \frac{k_B}{2} \ln \det\left[1 + \frac{k_B T e^2}{\hbar^2}\underline{\mathbf{D}}\right] \qquad (1)$$

where $k_B$ is Boltzmann's constant, $T$ is the absolute temperature, $e$ is Euler's number, and $\hbar$ is Planck's constant divided by $2\pi$. Here, $\underline{\mathbf{D}}$ is the covariance matrix of mass-weighted atomic Cartesian coordinates, defined as

$$\underline{\mathbf{D}} = \langle[\underline{\mathbf{M}}^{1/2}(\mathbf{r} - \langle\mathbf{r}\rangle)] \otimes [\underline{\mathbf{M}}^{1/2}(\mathbf{r} - \langle\mathbf{r}\rangle)]\rangle \qquad (2)$$

where $\mathbf{r}$ is the $3N$-dimensional Cartesian coordinate vector of the $N$ particles (atoms or beads) considered for the entropy calculation after least-squares fitting onto a reference structure, $\underline{\mathbf{M}}$ is the $3N$-dimensional diagonal matrix containing the masses of these particles, $\langle ... \rangle$ denotes ensemble averaging, and the notation $\mathbf{a} \otimes \mathbf{b}$ stands for the matrix with elements $\mu,\nu$ equal to $a_\mu \cdot b_\nu$. For all systems considered, the initial system configurations (after equilibration) were used as reference to perform the structural least-squares fitting of trajectory configurations.

To define the notation unambiguously, the symbol $S_{\text{fit}}^{\text{type}}(\text{cov})$ will be used to denote the entropy estimated from the covariance matrix for the set of $N$ particles defined by the cov reference code, using a least-squares fit of trajectory configurations based on the set of particles defined by the fit reference code, while the type reference code indicates how the fitting procedure is performed. Atoms in the fit set may be the same as those in the cov set, but they may also differ. In the present work, the cov set is always identical to or a subset of the fit set. In practice, two alternative sets of particles were used to define cov and fit as summarized in Table 2, namely, (i) the entire alkane or alkene chain of a particular hydrocarbon molecule (reference code ch) or (ii) a fragment of the hydrocarbon chain (reference code fc; see, e.g., Figure 1).

**TABLE 2: Reference Code Definitions for the Particle Sets Used in Estimating the (Single-Molecule or Single-Fragment; Internal or Internal Plus Rotational) Configurational Entropy $S_{\text{Fit}}^{\text{Type}}(\text{cov})$[a]**

| type | description |
|---|---|
| *i* | internal configurational entropy (overall translation and rotation removed) |
| *ir* | internal plus rotational configurational entropy (overall translation removed) |
| *r* | rotational entropy contribution (eq 3) |
| ip | internal configurational entropy per particle |
| irp | internal plus rotational configurational entropy per particle |
| **fit and cov** | **description** |
| ch | complete alkane or alkene chain |
| fc | fragment of the chain |

[a] A reference code is given for the type of estimate (type), the sets of atoms used for the fitting (fit), and the mass-weighted covariance matrix calculation (cov). See the Methods section for definitions.

To investigate the separate contributions of internal and rotational degrees of freedom to the entropy, two alternative fitting procedures were used in the superposition of successive trajectory structures onto the reference one, as summarized in Table 2 (type reference code). In the first one, the molecular configurations were superposed via a translational superposition of centers of mass followed by a rotational least-squares fit,[39] thus excluding the rotational motion from the calculated (single-molecule or single-fragment) configurational entropies.[25] This yields an internal (type: i) or internal per particle (type: ip) entropy (the latter quantity being the entropy divided by the number $N$ of particles in the cov set). In the second one, a translational superposition was performed without applying any rotational transformation, thus including the rotational motion in the calculated (single-molecule or single-fragment) configurational entropies. This yields an internal plus rotational (type: ir) or internal plus rotational per particle (type: irp) entropy.

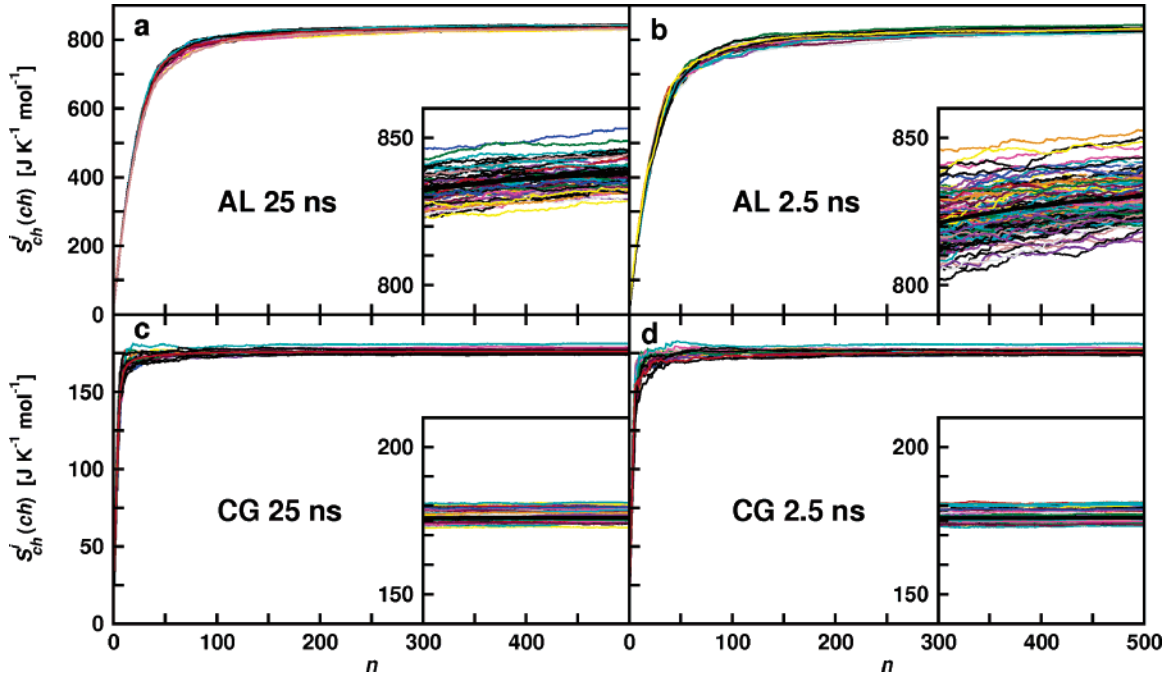


**Figure 2.** Single-molecule internal configurational entropies $S^{i}_{ch}(ch)$ as a function of the number $n$ of configurations included in the estimate, for hexadecane (C16). The estimated entropies are displayed for a randomly chosen set of 16 out of 128 molecules (colored lines) as calculated based on $n = 0...500$ time-equidistant configurations collected from a 25 ns (a and c) or a 2.5 ns (b and d) simulation period with the atomic-level (AL; a and b) or the coarse-grained (CG; b and d) model. The curves averaged over the 128 molecules are also displayed (thick black lines). The curves for all 128 simulated chains are shown in scaled insets over the range $n = 300...500$. Error bars are smaller than 0.5 J K$^{-1}$ mol$^{-1}$ (not displayed). See Table 2 and the Methods section for definitions of the entropy codes.

The relative contribution of overall rotation $s^{r}_{fit}(cov)$ to the total entropy (expressed in percent) may be estimated from the difference between the entropies calculated using the two fitting procedures, i.e., as

$$s^{r}_{fit}(cov) = \frac{S^{ir}_{fit}(cov) - S^{i}_{fit}(cov)}{S^{ir}_{fit}(cov)} \times 100 \qquad (3)$$

The reported configurational entropy estimates are the average values of the (single-molecule or single-fragment; see Table 1) configurational entropies over the set of molecules simulated, unless otherwise specified. Corresponding error bars are evaluated as twice the standard deviation around the average.

## Results and Discussion

**Convergence of the Single-Molecule Entropies in Atomic-Level and Coarse-Grained Models.** Cumulative estimates of the single-molecule internal configurational entropy ($S^{i}_{ch}(ch)$; see Table 2 for reference codes) for hexadecane (C16) treated with either the atomic-level (AL) or coarse-grained (CG) model are displayed in Figure 2 as a function of the number $n$ of (time-equidistant) configurations used in the estimate and based on two different simulation periods. In Figure 2a and b, the build-up curves are displayed for a set of 16 chains taken from a system consisting of 128 AL C16 molecules simulated for 25 or 2.5 ns at 323 K. The build-up curve averaged over all simulated hydrocarbon chains is also drawn. The curves are found to be very similar for all chains, although the spread of configurational entropies among the 128 simulated molecules (insets in Figure 2a and b) is significantly larger when the estimate is based on the shorter simulation period of 2.5 ns (compared to 25 ns). However, in both cases, the spread is small relative to the final average entropy value and decreases upon increasing the number of configurations considered in the entropy evaluation. Convergence of the average build-up curve to 99% of its final estimate (for 500 configurations) is reached with 264 and 314 configurations for the simulation periods of 25 and 2.5 ns, respectively. The corresponding build-up curves are displayed in Figures 2c and d for comparable simulations performed with the CG model of C16 (128 chains simulated at 323 K). The entropy estimates based on the CG model require much fewer configurations to reach convergence, namely 59 or 63 configurations to account for 99% of the final estimate for the simulation periods of 25 and 2.5 ns, respectively. This indicates that the accessible conformational space of the CG C16 chains is sampled much faster compared to that of AL C16 chains, which is not surprising considering that one CG bead represents four AL atoms. The spread of entropy values among the 128 molecules (insets in Figures 2a−d) is smaller in the CG model compared to the AL model, i.e., the distribution of entropy values over the C16 chains is wider in the AL representation. A very similar behavior is found for *cis*-9-octadecene (C18:c9) chains in both the AL and CG models (data not shown).

A more detailed analysis of the configurational entropy is given in Table 3, which reports internal $S^{i}_{ch}(ch)$ as well as internal plus rotational $S^{ir}_{ch}(ch)$ single-molecule configurational entropies for liquid C16 in the AL and CG models for different simulation periods, different numbers of configurations used in the entropy estimate, and different reference temperatures. For practical purposes, entropy differences smaller than 2% are considered to be negligible, because of the limited intrinsic accuracy of the method. Expectedly, both $S^{i}_{ch}(ch)$ and $S^{ir}_{ch}(ch)$ noticeably increase upon raising the simulation temperature, for all systems and in both representations, the sensitivity to the temperature being larger in the AL model compared to the CG one. Comparatively smaller increases are observed upon increasing the time period used for estimating the entropy. The

**TABLE 3: Experimental Molecular Entropies and Calculated Single-Molecule Configurational Entropies from MD Simulations of Liquid Hydrocarbons[a]**

| | exp[d] | calculated | | | | | | | | |
|---|---|---|---|---|---|---|---|---|---|---|
| molecule | $S^{exp}_{liquid}$ | $S^{i}_{ch}$(ch) | $S^{ir}_{ch}$ (ch) | $S^{ip}_{ch}$(ch) | $S^{irp}_{ch}$(ch) | no. atoms in fit | $S^{r}_{ch}$(ch) (%) | time period (ns) | no. configs | $T$ (K) |
| | | | | | AL model | | | | | |
| dodecane | 491[e] | 519 | 699 ± 1 | 43 | 58 | 12 | 26 | 2.5 | 1000 | 303 |
| tetradecane | 555[e] | 630 | 813 | 45 | 58 | 14 | 22 | 2.5 | 1000 | 303 |
| hexadecane[b] | 606[f] | 830 | 1032 | 51 | 63 | 16 | 18 | 2.5 | 500 | 323 |
| | | 838 | 1041 | 52 | 65 | 16 | 19 | 25 | 500 | 323 |
| | | 824 | 1028 | 51 | 64 | 16 | 20 | 200 | 1000 | 303 |
| | | 842 | 1045 | 53 | 65 | 16 | 19 | 200 | 1000 | 323 |
| | | 859 | 1061 | 54 | 66 | 16 | 19 | 200 | 1000 | 343 |
| octadecane | 697[g] | 970 | 1178 | 54 | 65 | 18 | 18 | 25 | 1000 | 323 |
| *cis*-9-octadecene[c] | | 935 | 1143 | 52 | 63 | 18 | 18 | 25 | 1000 | 303 |
| | | | | | CG model | | | | | |
| hexadecane[b] | | 176 | 335 | 44 | 84 | 4 | 47 | 2.5 | 1000 | 303 |
| | | 176 | 338 | 44 | 84 | 4 | 48 | 25 | 1000 | 303 |
| | | 179 | 339 | 45 | 85 | 4 | 47 | 2.5 | 1000 | 323 |
| | | 179 | 341 | 45 | 85 | 4 | 47 | 25 | 1000 | 323 |
| *cis*-9-octadecene[c] | | 275 | 452 | 55 | 90 | 5 | 39 | 1000 | 2500 | 303 |
| | | 280 | 456 | 56 | 91 | 5 | 38 | 1000 | 2500 | 323 |

[a] Values of the standard deviation around the average (over all molecules) are only reported when larger than 0.5 J $K^{-1}$ $mol^{-1}$. Entropies are calculated using different numbers of configurations collected over simulation periods of different lengths. The number of atoms used for the fitting procedure, the relative contribution of overall rotation to the absolute entropy, and the simulation temperature are also reported. See Table 2 and the Methods section for configurational entropy nomenclature. [b] Results are averaged over the 128 alkane chains simulated. [c] Results are averaged over 128 chains among the 512 alkene chains simulated. [d] Experimental data at 298 K from heat capacity measurements. [e] Reference 40. [f] Averaged from refs 40 and 41. [g] Reference 41.

relative contribution $s^{r}_{ch}$(ch) of overall rotation to the configurational entropy of C16 chains does not significantly vary with temperature and represents about 19% and 47% of the total single-molecule (internal plus rotational) entropy for the AL and CG models, respectively.

To assess the convergence of the entropy with respect to different molecules, single-molecule configurational entropies of C16 in the AL model at 323 K were estimated from the concatenated trajectories (each 200 ns in length) of 16 randomly chosen chains. Figure s1 shows the corresponding build-up curves of both the internal $S^{i}_{ch}$(ch) and internal plus rotational $S^{ir}_{ch}$(ch) entropies (see the Supporting Information). It appears that the concatenated trajectories of three distinct molecules are already sufficient to generate an ensemble of configurations accounting for more than 99% of the total internal configurational entropy $S^{i}_{ch}$(ch). A slightly larger number of four trajectories is necessary to also adequately sample the accessible rotational space and account for 99% of the internal plus rotational entropy $S^{ir}_{ch}$(ch). Both configurational entropies calculated from the ensembles of 16 concatenated trajectories are very well converged, which is not surprising considering that these estimates are based on a total simulation time of 3.2 $\mu$s. The configurational entropy estimates are completely independent of the chronological order in which the different trajectories are concatenated (results not shown), which is a direct consequence of the definition of configurational entropy as a thermodynamic state quantity. In the case of AL C16 at 323 K, $S^{i}_{ch}$(ch) and $S^{ir}_{ch}$(ch) are estimated to be 845 and 1050 J $K^{-1}$ $mol^{-1}$, respectively. These values agree very well with those obtained by averaging over all 128 alkane chains simulated for a period of 200 ns (Table 3), namely, 842 and 1045 J $K^{-1}$ $mol^{-1}$, confirming that the latter values are also well converged.

**Single-Molecule Configurational Entropies vs Experimental Molecular Entropies.** Experimental molecular entropies derived from temperature integration of the measured heat capacity[40,41] are reported in Table 3. Direct comparison between experimental molecular entropies and calculated single-molecule configurational entropies is of limited value for a number of reasons (Table 1): (i) single-molecule translational entropy contributions (based on the liquid density at a standard pressure of 1 bar) are encompassed in the experimental values but are absent in the calculated ones; (ii) single-molecule rotational entropy contributions are encompassed in the experimental values but are absent in ($S^{i}_{ch}$(ch)) or overestimated ($S^{ir}_{ch}$(ch)) in the calculated ones; (iii) the calculated (quasi-harmonic) single-molecule entropies neglect contributions from mode anharmonicity, (supralinear) pairwise mode correlations and all higher-order correlations;[30] (iv) intermolecular correlations among hydrocarbon chains (involving translational, rotational, and internal degrees of freedom of the individual chains) contribute to the experimental molecular entropies, but not to the calculated single-molecule entropies; (v) experimental and theoretical values correspond to slightly different temperatures. If the calculated values for $S^{i}_{ch}$(ch) could be corrected for these effects (so as to reach an estimate comparable with experimental molecular entropies), the correction terms for effects i and ii would be positive and those for effects iii and iv would be negative, while approximation v is of minor relevance in view of the limited temperature dependence of the calculated entropies (Table 3). On the basis of $S^{ir}_{ch}$(ch), the correction term for effect ii would be negative instead. The observation that theoretical single-molecule values (either $S^{i}_{ch}$(ch) or $S^{ir}_{ch}$(ch)) are found to be systematically higher than the experimental molecular values suggests that the neglect of anharmonicity, mode correlation, and intermolecular correlations is the main cause for the observed differences.

Despite these limitations, trends in the experimental and calculated entropies may be compared. For example, both sets of values for pure liquid hydrocarbons expectedly increase with increasing chain length. This dependence agrees with the experimentally observed increase in the molar heat capacity $C_{p,m}$ upon increasing the hydrocarbon chain length.[42] The same trend is displayed by the calculated per particle values. It is also interesting to note that there exists a linear relationship between

the molecular radius of gyration (averaged over the 128 simulated hydrocarbon molecules) and the inverse of the relative contribution of rotational entropy to the total entropy (Figure s2, linear correlation coefficient is 0.99, calculated considering all *n*-alkanes).

To analyze in more detail the relationship between experimental measurements and calculations, the heat capacity was estimated from three simulations (1000 configurations collected over a simulation period of 200 ns) of 128 AL or CG C16 at 303, 323, and 343 K (Table 3). From these simulations, the constant-pressure molar heat capacity can be calculated in two ways based on standard thermodynamic relationships between two system states A and B.[43] First, it can be evaluated as

$$C^{H}_{p,m} = \frac{H(T_B) - H(T_A)}{T_B - T_A} \quad (4)$$

where $H = \langle U \rangle + P\langle V \rangle$ is the molar enthalpy of the system at the given temperature and pressure. Second, it can be evaluated as

$$C^{S}_{p,m} = \frac{S(T_B) - S(T_A)}{\ln(T_B/T_A)} \quad (5)$$

where $S$ is the molar entropy, this equation following from integrating $C_{p,m} = T(\partial S/\partial T)_P$ with the assumption of a constant heat capacity in the given temperature range. These values can be compared to the experimental molar heat capacity $C^{exp}_{p,m}$(323.15 K,1 bar) = 516 J K$^{-1}$ mol$^{-1}$ for hexadecane.[42] Using eq 4, one finds the values $C^{H}_{p,m}$(323 K,1 bar) = 273 and 103 J K$^{-1}$ mol$^{-1}$ for the AL and CG models, respectively. The value for the AL model is expected to be comparable with experiment values (neglecting the possible contribution of the CH bonds, absent in the united-atom representation), because the enthalpy accounts for intermolecular correlations. The $P\langle V \rangle$ term was found to be of negligible magnitude; errors are not reported for this qualitative comparison. Using eq 5 together with the single-molecule configurational entropies $S^{i}_{ch}$(ch) reported in Table 3, one finds $C^{S}_{p,m}$(323 K,1 bar) = 282 and $C^{S}_{p,m}$(313 K,1 bar) = 282 J K$^{-1}$ mol$^{-1}$ for the AL model, and $C^{S}_{p,m}$(313 K,1 bar) $\simeq$ 47 J K$^{-1}$ mol$^{-1}$ for the corresponding CG model (the corresponding experimental value extrapolated[42] for 313 K being $C^{exp}_{p,m}$(313.15 K,1 bar) = 509 J K$^{-1}$ mol$^{-1}$). However, because the value for $C^{S}_{p,m}$ is based on approximate (quasi-harmonic) entropies that neglect the contribution of molecular translation and rotation as well as intermolecular correlations, it is not directly comparable with those for $C^{H}_{p,m}$ and $C^{exp}_{p,m}$. The large decrease in the heat capacity between the AL and CG models is due to the reduced number of degrees of freedom in the CG model.

Equations 4 and 5 can also be combined to provide an estimate of the entropy change upon increasing the temperature

$$\Delta S^{H} = S(T_B) - S(T_A) \approx \frac{[H(T_B) - H(T_A)]\ln(T_B/T_A)}{T_B - T_A} \quad (6)$$

This equation was applied to estimate the change in molecular entropy (including the effect of molecular translation and rotation, as well as intermolecular correlations) for a system of 128 AL C16 chains using the total energies from simulations at 303, 323, and 343 K. The resulting estimated changes in molecular entropy are $\Delta S$(303 K $\rightarrow$ 323 K) = 8 $\pm$ 4, $\Delta S$(323 K $\rightarrow$ 343 K) = 7 $\pm$ 4, and $\Delta S$(303 K $\rightarrow$ 343 K) = 15 $\pm$ 4 J K$^{-1}$ mol$^{-1}$. These values can be compared with the corresponding changes in single-molecule configurational entropies derived from the data in Table 3. These changes are $\Delta S^{i}$(303 K $\rightarrow$ 323 K) = 18, $\Delta S^{i}$(323 K $\rightarrow$ 343 K) = 17, $\Delta S^{i}$(303 K $\rightarrow$ 343 K) = 35, $\Delta S^{ir}$(303 K $\rightarrow$ 323 K) = 17, $\Delta S^{ir}$(323 K $\rightarrow$ 343 K) = 16, and $\Delta S^{ir}$(303 K $\rightarrow$ 343 K) = 33 J K$^{-1}$ mol$^{-1}$, in terms of single-molecule internal and internal plus rotational entropies. The correspondence between these and the above estimates for the molecular entropy change suggests that the leading contribution to these changes (in the temperature range considered) is due to single-molecule contributions, while the corresponding changes in the translational, rotational, and intermolecular contributions are comparatively small.

To investigate the effect of the solvent environment, the single-molecule $S^{i}_{ch}$(ch) and $S^{ir}_{ch}$(ch) of a single C16 chain in a vacuum were estimated from a 200 ns simulation at 323 K with solute degrees of freedom weakly coupled to an external thermal bath[36] (relaxation time 0.1 ps) based on 1000 trajectory structures. The results (directly comparable to the MD results for the liquid phase reported in Table 3), $S^{i}_{ch}$(ch) = 858 and $S^{ir}_{ch}$(ch) = 1057 J K$^{-1}$ mol$^{-1}$, are only 2 and 1% larger than the corresponding ones for MD of C16 in the liquid phase (Table 3). The small difference can be explained considering that the configurational entropy of a single solute molecule is affected by the surrounding environment. The decrease of single-molecule configurational entropy upon going from the gas to the liquid phase is due to the restriction of the chain flexibility due to interaction with neighboring chains in the liquid phase.

**Flexibility of Liquid Hydrocarbon Chains.** The distribution of configurational entropy along the hydrocarbon chains was also determined for the set of hydrocarbons considered. The calculations were based on a subdivision of the aliphatic chain into fragments (fc), as illustrated in Figure 1 for C16 and C18:c9. Fragments of 4 methylene groups were chosen because the CG model maps the same subgroups of atoms of the AL model to a single bead. Figure 3 shows the single-fragment internal and internal plus rotational configurational entropies per particle, $s^{ip}_{ch}$(fc) and $S^{irp}_{ch}$(fc), for the set of hydrocarbons investigated. Expectedly, the latter values are always larger than the former ones, because they (approximately) encompass the rotational entropy contribution for the fragment. However, similar distributions are observed for the two quantities $s^{ip}_{ch}$(fc) and $S^{irp}_{ch}$(fc) (with only the exception of C18:c9, see below). The entropy is larger for the fragments in the terminal parts of the chains compared to the corresponding central fragments, indicating that the former are comparatively more flexible than the latter. The curves are also symmetrical with respect to the middle of the chain, as expected for a sufficient sampling of the accessible configurational space (i.e., adequate convergence of the entropy calculations). For C18:c9, the internal configurational entropy of the central fragment is significantly lower compared to C18 due to the presence of the central double bond in this fragment. This bond confers a higher degree of rigidity to the two neighboring fragments (cf. C18 and C18:c9 fragments with central atom sequence numbers 6 and 12 in Figure 3). In contrast, the internal entropy estimates for the two terminal fragments are similar for C18 and C18:c9. The distribution of internal plus rotational $S^{irp}_{ch}$(fc) configurational entropy for C18:c9 follows the same trend as that of the internal configurational entropy, except for the central fragment. This more rigid fragment is found to provide a large contribution to the rotational entropy, even if its internal contribution is reduced. This observation suggests that the central part of the chain experiences rotational motions which are not strictly depending on

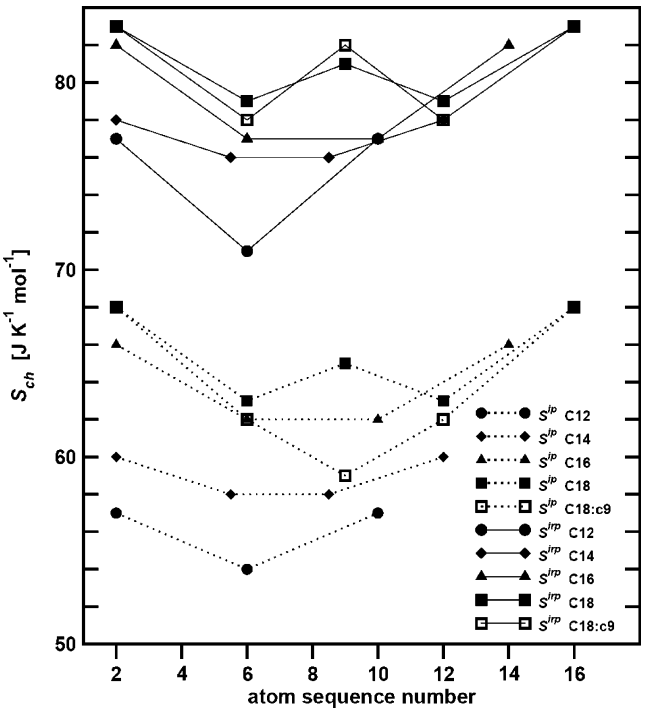


**Figure 3.** Internal $S_{ch}^{ip}$(fc) and internal plus rotational $S_{ch}^{irp}$(fc) configurational entropies per particle for different liquid hydrocarbons calculated for fragments along the chain based on the AL model at temperatures specified in Table 3. Fragment entropies are displayed as a function of the atom sequence number along the alkane chain. Error bars are smaller than 0.5 J K$^{-1}$ mol$^{-1}$ (not displayed). The lines are meant to guide the eye. See Table 2 and the Methods section for definitions of the entropy codes.

its flexibility. Estimates of $S_{ch}^{i}$(fc) and $S_{ch}^{ir}$(fc) for the other hydrocarbons considered in the present study are given in Table s1.

**Comparison of Atomic-Level and Coarse-Grained Models.** Configurational internal plus rotational entropies based on the AL and CG models are compared in Table 4 on a fragment (AL) or bead (CG) basis. A third set of entropies corresponds to a CG representation derived from the trajectory simulated using the AL model, in which the center of mass of each fragment is mapped to a bead (MAP). Note that the AL entropies involve (translational) superposition of trajectory configurations based on the individual fragment, while the superposition is based on the whole chain for the CG and MAP cases. Results for CG C16 and CG C18:c9 are directly comparable (although they were calculated from simulations of different time lengths and using different numbers of configurations), because complete convergence was reached in both cases for the corresponding $S_{fc}^{ir}$(fc) entropies (not shown). The MAP and CG results are directly comparable (i.e., they can be used to assess the compatibility between the AL and CG models, in terms of sampling of configurational space and flexibility). The CG model clearly provides a reasonable description of the overall hydrocarbon chain flexibility with reference to the AL model (in its mapped form) for both C16 and C18:c9. The agreement is slightly better for C16 compared to C18:c9 chains, the latter being more flexible around the central part in the CG model compared to the AL model (in its mapped form). This small discrepancy between AL and CG models could probably be reduced by using a slightly stiffer bond-angle potential around the central bead of CG C18:c9.

The comparison of the AL and MAP results provides an indication of the loss in configurational entropy upon coarse-graining the AL model. This entropy loss depends on the fragment position along the chain. This may be a consequence of the fact that back-folding of the chain ends occurs to a larger extent in the AL model than in the CG model, because (i) the CG beads are larger than the corresponding AL united-atom particles and (ii) back-folding requires large deviations from the equilibrium angles in the CG model but can be achieved through a number of comparatively smaller deviations of bond angles and torsional angles in the AL model. It can also be noticed that the entropy loss is comparatively larger for C16 than for C18:c9. This is because, in the former molecule, the coarse-graining reduces the original 16 united atoms to 4 beads, while, in the second, the reduction is from 18 to 5, so that the ratio between the number of degrees of freedom in the CG and AL models is larger in this latter case.

**TABLE 4: Comparison between the Atomic-Level (AL) and Coarse-Grained (CG) Models for Hydrocarbon Chains in Terms of Single-Fragment (or Bead) Configurational Entropies**[a]

| | | $S_{fc}^{ir}$(fc) | $S_{ch}^{ir}$(fc) (J K$^{-1}$ mol$^{-1}$) | $S_{ch}^{ir}$(fc) |
|---|---|---|---|---|
| system | *fc* | AL | MAP | CG |
| hexadecane[b] | A | 211 | 133 | 131 |
| | B | 209 | 111 | 110 |
| | C | 209 | 111 | 110 |
| | D | 211 | 133 | 131 |
| *cis*-9-octadecene[c] | A | 211 | 135 | 136 |
| | B | 209 | 117 | 121 |
| | C | 66 | 101 | 108 |
| | D | 209 | 117 | 121 |
| | E | 211 | 135 | 136 |

[a] Standard deviations around the average are smaller than 0.5 J K$^{-1}$ mol$^{-1}$. For a direct comparison, the configurational entropy is also calculated based on the centers of mass of single-fragments in the AL model, which map onto corresponding coarse-grained beads (MAP). Fragment (*fc*) nomenclature refers to Figure 1. See Table 2 and the Methods section for definitions of the entropy codes. [b] AL and MAP data is from 25 ns MD simulation at 323 K (500 configurations used). CG data is from 1 $\mu$s MD simulation at 323 K (2500 configurations used). [c] AL and MAP data is from 25 ns MD simulation at 303 K (500 configurations used). CG data is from 2.5 $\mu$s at 303 K (2500 configurations used). Note: fragment C only includes 2 united atoms, which map onto one specific bead in the CG model.

Vaporization enthalpies ($\Delta H_{vap}$) were also calculated from (N,p,T) ensembles as previously described[32,34] and used for comparison of the two models. From simulations of C16 (AL 2 ns; CG 30 ns) at 303 K, we find $\Delta H_{vap}^{AL} = 80$ and $\Delta H_{vap}^{CG} = 66$ kJ mol$^{-1}$. Vaporization thermodynamic analysis is being pursued in more detail elsewhere.

Conformational analysis was performed for C16 and C18:c9 in terms of pseudo-bond angles and pseudo-torsional angles between mapped fragments (AL model) or beads (CG model). The corresponding normalized distributions averaged over all the 128 simulated molecules are displayed in Figure 4. For C16, a good correspondence is found between AL and CG pseudo-bond angle distributions (A−B−C and B−C−D). The agreement is not as good for the pseudo-torsional angle (A−B−C−D), where the normalized distribution for the CG model shows a uniform sampling, while the corresponding AL model (in its mapped form) shows a bias toward low angles. This observation can be explained considering that in the CG model no dihedral-angle potential is applied, in contrast to the AL model. For C18:c9, a good correspondence is observed between the two sets of normalized distributions (except for a slight shift in the peak position for the B−C−D pseudo-bond angle). For both C16 and C18:c9, the CG model displays only slightly narrower

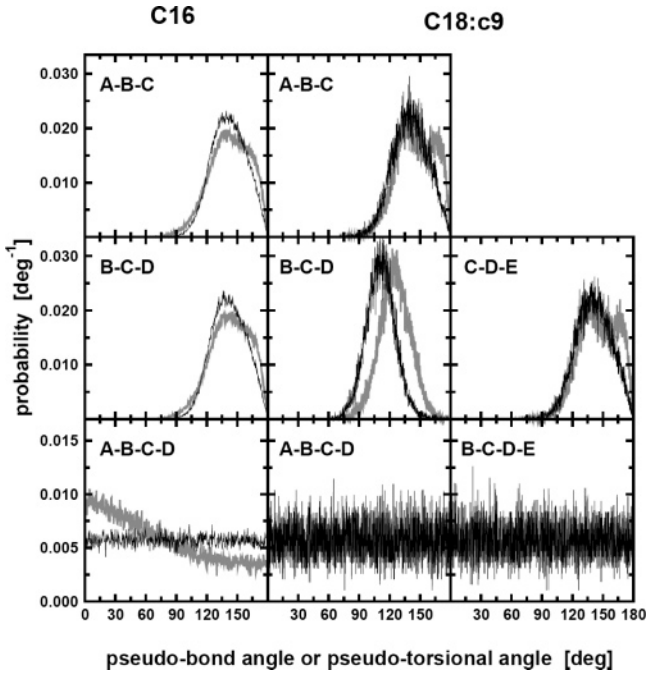


**Figure 4.** Normalized probability distributions of pseudo-bond and pseudo-torsional angles from simulations (AL 25 ns; CG 1 $\mu$s) of liquid hexadecane (C16) at 323 K and liquid *cis*-9-octadecene (C18:c9) at 303 K, defined based on mapped beads (MAP; grey lines) or beads (CG model; black lines). Mapped beads refer to the centers of mass of the AL fragments. All 128 simulated C16 chains were used to calculate the averaged normalized distributions. Fragment and bead nomenclature refers to Figure 1.

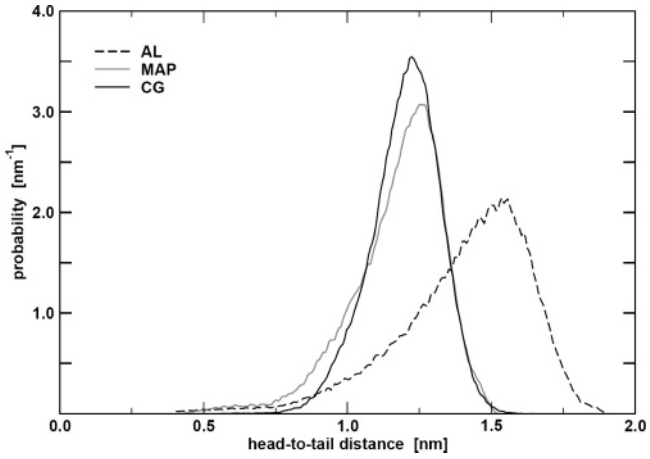


**Figure 5.** Normalized probability distributions of head-to-tail distance from simulations (AL 25 ns; CG 1 $\mu$s) of liquid hexadecane (C16) at 323 K, defined based on the two terminal united atoms (AL model; dashed black line), the two terminal mapped beads A and D (MAP; grey line), or beads A and D (CG model; solid black line). Mapped beads refer to the centers of mass of the AL fragments. All 128 simulated C16 chains were used to calculate the averaged normalized distributions. Fragment and bead nomenclature refers to Figure 1.

pseudo-bond angle distributions compared to the AL model (in its mapped form), despite the reduced number of degrees of freedom.

Differences between the AL and CG models were further analyzed for C16 by calculating distributions of the head-to-tail distance. The results are shown in Figure 5. Similar distributions are found for the AL (MAP form) and CG trajectories, with peaks centered at about 1.2 nm. The distribution of the fragment centers of mass in the AL model (MAP) is slightly shifted toward shorter distances compared to the

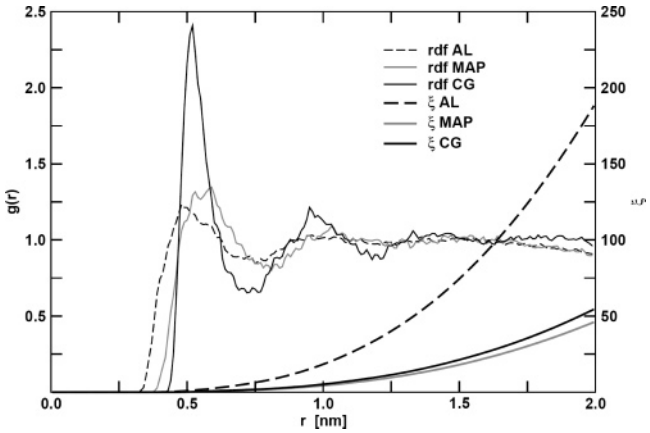


**Figure 6.** Radial distribution functions (rdf) $g(r)$ and their integrals from (AL 25 ns; CG 1 $\mu$s) simulations of liquid hexadecane (C16) at 323 K, defined based on the two terminal united atoms (AL model; dashed black line), the two terminal mapped beads A and D (MAP; grey line), or beads A and D (CG model; solid black line). The functions (rdf; thin lines) were calculated taking into account all united atoms, mapped beads, or beads excluding intramolecular pairs. The corresponding running integrals $\xi$ of $4\pi r^2\rho g(r)$ are also shown (thick lines). Mapped beads refer to the centers of mass of the fragments. Fragment (bead) definition refers to Figure 1.

distribution of CG beads, which is due to the internal flexibility of the four-atom fragments in the AL model. The distribution for the AL model is broader and shifted by 0.3 nm toward larger distances. This is not unexpected since the distance between the center of mass of a fragment and one of its outer atoms is about 0.19 nm.

Finally, the general structural properties of the liquid in the AL and CG models were compared by calculating three different types of radial distribution function (rdf) for C16: (i) for the carbon-atom coordinates (AL model), (ii) for the coordinates of the centers of mass of the AL fragments (MAP), and (iii) for the CG beads (CG). Rdfs for the atoms (AL) or beads (CG) from one randomly chosen molecule were calculated based on 1000 trajectory structures of C16 at 323 K, excluding the neighboring carbon atoms (AL) or beads (CG) of the same molecule. The results are shown in Figure 6. The CG model evidences stronger ordering (higher peak) than the AL and MAP models, especially in the first coordination shell. However, the number of particles in this first shell (about 6) is almost the same in the three cases as observed from the rdf integrals. Additionally, a slightly larger number of particles coordinated at 2.0 nm for the CG liquid with respect to the MAP one is observed, corresponding to a higher liquid density (an observation which agrees with previously reported liquid densities for the AL[32] and CG[1] models). Differences between the CG and MAP models that may directly affect the rdfs are the following: (i) the size of one CG bead (0.47 nm in diameter) is constant during the simulation, while fragments of four AL methylene groups have a variable size; (ii) the CG model does not involve constraints for the distances but rather harmonic springs between consecutive beads; and (iii) the AL force field excludes Lennard−Jones interactions up to second nearest neighbors, while the CG force field restricts the exclusion to first neighbors.

## Conclusions

In the present work, the properties of liquid hydrocarbons have been investigated using models at two different resolution scales, namely, atomic-level (AL) and coarse-grained (CG)

models. The following main conclusions can be drawn from this study:

(A) The values of single-molecule configurational entropies based on molecular dynamics (MD) simulations using the quasi-harmonic approach may depend significantly on the simulation period considered and on the number of structures used to estimate the configurational entropy. For the set of hydrocarbons considered, the sampling of internal motion is reached on a time period of tens of nanoseconds (based on 500 structures or more) for both AL and CG models. In the latter case, the reduced number of degrees of freedom allows convergence to be reached from even shorter simulations. On the contrary, the rotational contributions, (qualitatively) captured in the internal plus rotational single-molecule entropy, require comparatively longer simulations to reach complete convergence.

(B) A comparison between single-molecule configurational entropies and (experimentally accessible) molecular entropies is difficult. While the first quantity can be estimated by MD simulations within the limits of the quasi-harmonic approximation, the second (including the diffusive degrees of freedom and the effect of intermolecular correlations) is currently difficult to access by simulation. However, the temperature dependences of the two quantities, related to the corresponding molar heat capacities, appear to be comparable (AL model vs experiment) in the limited temperature range considered. This temperature dependence is found to be weaker in the case of the CG model.

(C) The loss of configurational entropy upon coarse-graining the simulation model AL to CG can be estimated by comparing AL atomic trajectories to corresponding bead trajectories (MAP) obtained by mapping fragment centers of mass to one bead based on the same trajectories. For hexadecane and *cis*-9-octadecene, the entropy loss upon coarse-graining (which depends on the fragment position along the chain) is found to be on the order of $40-100\ \mathrm{J\ K^{-1}\ mol^{-1}}$ per bead and to be systematically higher for hexadecane than *cis*-9-octadecene.

(D) The CG model provides a good description of the overall hydrocarbon chain flexibility with reference to the AL model (MAP form) for the hydrocarbons considered. In the case of *cis*-9-octadecene, the CG model could be further improved by using a slightly stiffer pseudo-bond angle potential for the central bead corresponding to the AL double bond. A reasonable agreement between the two levels of resolution (MAP vs CG) was met for all structural properties investigated (i.e., pseudo-bond angle and pseudo-torsional angle distributions, head-to-tail distance distributions, and distribution functions in the liquid phase). The different nature of the two force fields considered affects short-range local properties to a larger extent than it does long-range averaged ones. Indeed, the latter are those properties of interest for large-size system and/or long-timescale simulations the CG model has been designed for.

The present work represents a first step in the comparison of the AL and CG models in the context of lipids (the main target of the CG force field by Marrink et al.[1]), the tails of which correspond to the hydrocarbon templates studied here. Although the present study supports a good correspondence between AL and CG force fields, a comparison of other thermodynamic properties (e.g., thermodynamic quantities related to vaporization and solvation) would be useful. Such investigation is of primary importance to define a nonarbitrary procedure for the parametrization of CG force fields and their extension to other chemical groups of biological relevance (e.g., amino acid residues and DNA base pairs), by using the match to experimental thermodynamic quantities as a general criterion.

**Acknowledgment.** Financial support from the National Center of Competence in Research (NCCR), Structural Biology, of the Swiss National Science Foundation (SNSF) is gratefully acknowledged. R. B. thanks S. J. Marrink for useful discussions on the CG model.

**Supporting Information Available:** Single-fragment configurational entropies (AL model) of the alkane chains from MD simulations of liquid hydrocarbons. Single-molecule internal entropies including and excluding rotational contributions for hexadecane (AL model). Correlation between entropy and radius of gyration for *n*-alkanes. This material is available free of charge via the Internet at http://pubs.acs.org.

## References and Notes

(1) Marrink, S. J.; de Vries, A. H.; Mark., A. E. *J. Phys. Chem. B* **2004**, *108*, 750.

(2) Baschnagel, J.; Binder, K.; Doruker, P.; Gusev, A. A.; Hahn, O.; Kremer, K.; Mattice, W. L.; Müller-Plathe, F.; Murat, M.; Paul, W.; Santos, S.; Suter, U. W.; Tries, V. Bridging the gap between atomistic and coarse-grained models of polymers: status and perspectives. In *Viscoelasticity, atomistic models, statistical chemistry*; Advances in Polymer Sciences; Springer-Verlag: Heidelberg, 2000; Vol. 152, p 41.

(3) Müller-Plathe, F. *ChemPhysChem* **2002**, *3*, 754.

(4) Kremer, K. *Macromol. Chem. Phys.* **2003**, *204*, 257.

(5) Shelley, J. C.; Shelley, M. Y. *Curr. Opin. Colloid Interface Sci.* **2000**, *5*, 101.

(6) Müller, M.; Katsov, K.; Schick, M. *J. Polym. Sci. B* **2003**, *41*, 1441.

(7) Smit, B.; Hilbers, P. A. J.; Esselink, K.; Rupert, L. A. M.; van Os, N. M.; Schlijper, A. G. *Nature* **1990**, *348*, 624.

(8) Smit, B.; Esselink, K.; Hilbers, P. A. J.; van Os, N. M.; Rupert, L. A. M.; Szleifer, I. *Langmuir* **1993**, *9*, 9.

(9) Tozzini, V. *Curr. Opin. Struct. Biol.* **2005**, *15*, 144.

(10) Goetz, R.; Lipowsky, R. *J. Chem. Phys.* **1998**, *108*, 7397.

(11) Groot, R. D.; Madden, T. J.; Tildesley, D. J. *J. Chem. Phys.* **1999**, *110*, 9739.

(12) Shelley, J. C.; Shelley, M. Y.; Reeder, R. C.; Bandyopadhyay, S.; Klein, M. L. *J. Phys. Chem. B* **2001**, *105*, 4464.

(13) Murtola, T.; Falck, E.; Patra, M.; Karttunen, M.; Vattulainen, I. *J. Chem. Phys.* **2004**, *121*, 9156.

(14) Srinivas, G.; Shelley, J. C.; Nielsen, S. O.; Discher, D. E.; Klein, M. L. *J. Phys. Chem. B* **2004**, *108*, 8153.

(15) Molinero, V.; Goddard, W. A., III *J. Phys. Chem. B* **2004**, *108*, 1414.

(16) Groot, R. D.; Rabone, K. L. *Biophys. J.* **2001**, *81*, 725.

(17) Shelley, J. C.; Shelley, M. Y.; Reeder, R. C. *J. Phys. Chem. B* **2001**, *105*, 9785.

(18) Marrink, S. J.; Mark, A. E. *J. Am. Chem. Soc.* **2003**, *125*, 11144.

(19) Marrink, S. J.; Mark, A. E. *J. Am. Chem. Soc.* **2003**, *125*, 15233.

(20) Faller, R.; Marrink, S. J. *Langmuir* **2004**, *20*, 7686.

(21) Karplus, M.; Kushick, J. *Macromolecules* **1981**, *14*, 325.

(22) Di Nola, A.; Berendsen, H. J. C.; Edholm, O. *Macromolecules* **1984**, *17*, 2044.

(23) Edholm, O.; Berendsen, H. J. C. *Mol. Phys.* **1984**, *51*, 1011.

(24) Schlitter, J. *Chem. Phys. Lett.* **1993**, *215*, 617.

(25) Schäfer, H.; Mark, A. E.; van Gunsteren, W. F. *J. Chem. Phys.* **2000**, *113*, 7809.

(26) Andricioaei, I.; Karplus, M. *J. Chem. Phys.* **2001**, *115*, 6289.

(27) Reinhardt, W. P.; Miller, M. A.; Amon, L. M. *Acc. Chem. Res.* **2001**, *34*, 607.

(28) Peter, C.; Oostenbrink, C.; van Dorp, A.; van Gunsteren, W. F. *J. Chem. Phys.* **2004**, *120*, 2652.

(29) Carlsson, J.; Åqvist, J. *J. Phys. Chem. B* **2005**, *109*, 6448.

(30) Baron, R.; van Gunsteren W. F.; Hünenberger, P. H. *ChemPhysChem*, submitted for publication.

(31) van Gunsteren, W. F.; Billeter, S. R.; Eising, A. A.; Hünenberger, P. H.; Krüger, P.; Mark, A. E.; Scott, W. R. P.; Tironi, I. G. *Biomolecular Simulation*: *The GROMOS96 Manual and User Guide*; vdf Hochschulverlag AG an der ETH Zürich and BIOMOS b.v.: Zürich, Groningen, 1996.

(32) Schuler, L. D.; Daura, X.; van Gunsteren, W. F. *J. Comput. Chem.* **2001**, *22*, 1205.

(33) Oostenbrink, C.; Villa, A.; Mark, A. E.; van Gunsteren, W. F. *J. Comput. Chem.* **2004**, *25*, 1656.

(34) Schuler, L. D.; van Gunsteren, W. F. *Mol. Simul.* **2000**, *25*, 301.

(35) van der Spoel, D.; van Buuren, A. R.; Apol, M. E. F.; Meulenhoff, P. J.; Tieleman, D. P.; Sijbers, A. L. T. M.; Hess, B.; Feenstra, K. A.;

Lindahl, E.; van Drunen, R.; Berendsen, H. J. C. *GROMACS User Manual*, version 3.1.1; Groningen, The Netherlands, 2002; http://www.gromacs.org/.

(36) Berendsen, H. J. C.; Postma, J. P. M.; van Gunsteren, W. F.; Di Nola, A.; Haak, J. R. *J. Chem. Phys.* **1984**, *81*, 3684.

(37) Hockney, R. W. *Methods Comput. Phys.* **1970**, *9*, 136.

(38) Hess, B.; Bekker, H.; Berendsen, H. J. C.; Fraaije, J. G. E. M. *J. Comput. Chem.* **1997**, *18*, 1463.

(39) McLachlan, A. D. *J. Mol. Biol.* **1979**, *128*, 49.

(40) Finke, H. L. *J. Am. Chem. Soc.* **1954**, *76*, 333.

(41) Parks, G. S.; Moore, G. E.; Renquist, M. L.; Naylor, B. F.; McClaine, L. A.; Fujii, P. S.; Hatton, J. A. *J. Am. Chem. Soc.* **1949**, *71*, 3386.

(42) Banipal, T. S.; Garg, S. K.; Ahluwalia, J. C. *J. Chem. Thermodyn.* **1991**, *23*, 923.

(43) Reif, F. Macroscopic parameters and their measurements. In *Fundamentals of statistical and thermal physics*; McGraw-Hill: Singapore, 1965 (int. ed. 1985); p 139.